JOURNAL OF CATALYSIS 138, 721–732 (1992)

CO Hydrogenation on PdCo/NaY Catalysts: Metal Phases and Product Selectivity

YUAN-GEN YIN, ZONGCHAO ZHANG, AND WOLFGANG M. H. SACHTLER

V. N. Ipatieff Laboratory, Center for Catalysis and Surface Science, Northwestern University, Evanston, Illinois 60208

Received May 13, 1992; revised June 29, 1992

NaY-encapsulated Pd–Co bimetal catalysts of various Co/Pd ratios and pretreatment conditions were used for carbon monoxide hydrogenation. Preparation conditions have an overwhelming effect on the active phases and the catalyst selectivity. In Pd/NaY and bimetal samples with very low extent of Co reduction, the formation of Pd carbide is detected by XRD. On these catalysts methane is formed when particles are very small, but after some agglomeration, methanol is the dominant primary product of CO hydrogenation, secondary reactions on strong Brønsted-acid sites lead to dimethyl ether and heavy hydrocarbons. In bimetal PdCo/NaY samples calcination and reduction conditions are critical for the formation of PdCo alloy particles, which prevents the formation of Pd carbide, and methane selectivity is high. A higher Co content of the alloy particles is obtained after reduction at high temperature; these samples show a signature reminiscent of Fischer-Tropsch catalysts.

I. INTRODUCTION

CO hydrogenation has been extensively studied in view of its importance for basic catalytic science and its potential for production of a liquid energy carriers from natural gas or coal. Of particular interest are zeolite-encapsulated metal catalysts, on account of the shape selectivity and stabilization of metal clusters in the accessible cages, as has recently been demonstrated with Pd/5A catalyst for this reaction (*1*).

Supported Pd is an attractive catalyst due to its high activity and selectivity to methanol synthesis under mild conditions (*2, 3*). Bifunctional Pd-zeolite catalysts are particularly intriguing in view of their potential to produce gasoline range iso-alkanes or aromatics as a result of the Brønsted acidity and the shape selectivity of zeolite microcavity (*4–6*). While a promotional effect on Pd-based catalysts has been reported for metals such as La (*3*), the effect on CO hydrogenation of reducible transition metals capable of forming alloys with Pd is not well studied. Guczi reported that supported PdFe bimetal particles of very low Fe concentration favor the formation of methanol (*7, 8*). Increased Fe loading leads to the formation of iron carbides which increase methane production. A recent study of PdNi bimetal catalysts in zeolite Y showed that the increased Ni reduction leads to increased methane selectivity, in accordance with the high methanation activity of Ni catalysts (*9*).

Monometallic Co catalysts are known for their high propensity to produce higher aliphatic hydrocarbons; activity and selectivity of Co in the Fischer–Tropsch synthesis are superior to those of Fe and Ni. The catalytic performance depends on the type of support (*10*), the preparation conditions, and the size of the metal particles. It has been reported that finely dispersed Co in zeolite Y is highly selective for C_4-alkenes (*11*).

Little is known however of the effects on catalysis of alloying Co with Pd, which is the main focus of the present study. Our objective is to relate catalytic data with physical characterization, in particular, the presence or absence of alloy and carbide

0021-9517/92 $5.00

phases. As it became clear during this work that the catalytic product pattern can be dramatically changed by subtleties in the preparation, such as exposing the calcined catalyst precursors to an atmosphere containing water vapor, the present report is confined to work where these conditions have been rigidly kept constant; i.e., after calcination all samples were exposed to a well-defined atmosphere for several days.

In the literature Co/zeolites catalysts are usually prepared by impregnation, because zeolite-encaged Co prepared by ion exchange is almost irreducible at practical temperatures; therefore, the catalytic activity is negligible (*12–14*). In recent work we have, however, succeeded in achieving significant reduction of Co^{2+} ions in Y zeolites which contained Pd as a second metal. An important prerequisite is the proximity of Co and Pd ions before reduction (*15*). A dramatic alloying effect of PdCo/NaY bimetal catalysts has been identified recently in neopentane conversion (*16*). In the present study only PdCo/NaY catalysts prepared by ion exchange have been used. Preparation conditions are chosen which maximize the fraction of Co reduced in the proximity of Pd, to probe the effects of the interaction of both metals in syngas conversion catalysis.

II. EXPERIMENTAL

All catalysts were prepared by ion exchange of NaY (LZ Y52), following the procedure described in a previous publication (*15*). $CoCl_2 \cdot 6H_2O$ (Specialty products of Johnson Matthey, Materials Technology UK, batch number S94354) and $Pd(NH_3)_4(NO_3)_2$ (99.99%, Aldrich Chem. Co., lot number 09211 LX MX) were used as Co and Pd precursors, respectively. In the preparation of bimetallic catalysts, Co was ion exchanged first, followed by washing with doubly distilled water, filtration and drying at room temperature, and calcination to 500°C in O_2. A second ion exchange was performed with dilute $Pd(NH_3)_4^{2+}$ solution. All catalysts in the present study were calcined either at 250 or 500°C for 2 hr after a programmed temperature increase from room temperature at 0.5°C/min. Calcination was always performed *ex situ* in order to avoid formation of metal oxides in the stainless-steel reactor, as such oxides might interfere with the CO hydrogenation catalysis. After calcination, the samples were exposed to a controlled atmosphere for several days in a desiccator above a saturated solution of NH_4Cl in water before being transferred to the microreactor. The catalysts were then flushed with He during heating to reduction temperature and subsequently reduced in H_2 for 60 min. The reduction temperature (T_R) was set to either 250 or 500°C for samples that were calcined at T_C = 500°C, and to 350°C for samples calcined at T_C = 250°C. CO hydrogenation was conducted in a down-flow fixed bed microreactor (Max II, Xytel Corp.) at 250°C and 10 bar; the composition of the synthesis gas was H_2/CO = 1 and a total gas space velocity of about 3600–4000 hr^{-1} was used. The conversions were kept below 1% with 0.3–0.8 g of catalysts. The product effluent was analyzed with an on-line HP 5890A gas chromatograph equipped with a cross-linked methyl silicone capillary column (∅, 0.2 mm; length, 50 m) and FID with He carrier gas. HP 3390A integrator was used to record and integrate GC peaks.

Powder X-ray diffraction was carried out using Ni-filtered Cu$K\alpha$ radiation at 40 kV and 25 mA with a Rigaku Geigerflex diffractometer. Step-scan data in the 2θ region were recorded from 37° to 50° with a 0.02° step and 10 sec counting time. All samples were studied *ex situ* in air at room temperature after the termination of the reaction. No other treatment was performed prior to X-ray study.

III. RESULTS

III-a. Reaction Studies

Samples will be identified by three parameters characterizing their preparation, viz., the calcination temperature T_C, the exposition to H_2O vapor, and the temperature T_R

of subsequent reduction. For samples with Co/Pd ratios ranging from 0 to 3, three sets of these parameters have been used: 500/H_2O/250, 500/H_2O/500, and 250/H_2O/350. Because the fraction of Co^{2+} ion reduction depends critically on T_C and T_R, whereas Pd is always completely reduced, the rate data will be expressed in mmol CO converted per mol of Pd per sec. Use of a conventional turnover frequency is not meaningful in the present study due to the severe agglomeration of metal particles during the reaction. In comparing catalysts of different compositions, we use an abbreviated notation: Pd_9Co_9, e.g., stands for an NaY-supported sample containing nine palladium atoms and nine cobalt atoms per unit cell of the zeolite. ICP was used to determine the loading of Pd and Co in the catalysts. For example, the Pd content of the Pd_9Co_9/NaY and Pd_9Co_3/NaY catalysts were analyzed to be 5.27 and 5.36 wt% respectively, while the Co content of the Pd_9Co_9/NaY and Pd_9Co_3/NaY were analyzed to be 2.70 and 1.01 wt%, respectively. For simplicity, the exact unit cell formulas $Pd_{8.8}Co_{8.2}$/NaY and $Pd_{8.9}Co_{3.1}$/NaY are expressed as Pd_9Co_9/NaY and Pd_9Co_3/NaY respectively.

III-a-1. 500/H_2O/250. The conversions and selectivities to methane, C_{2+}, and oxygenates for catalyst Pd_9, Pd_9Co_3, Pd_9Co_9, and Pd_3Co_9 calcined at 500°C and reduced at 250°C show some common features. While the initial activities of CO conversion of these catalysts differ considerably, these differences become insignificant at steady state after 2–4 hr. As an example, the activity pattern of Pd_9Co_9 is plotted in Fig. 1 against time on stream (TOS). Also the selectivities of the samples do not differ much. They all show a fairly rapid decline in methane formation with a steady increase in higher hydrocarbons (C_{2+}). In addition, the formation of methanol and dimethyl ether (designated as MeOH + DME hereafter) shows a small maximum at TOS of 1 hr and then decreases. It varies to a small extent for different Co/Pd ratio in the 500/H_2O/250 catalysts series. The selectivity changes

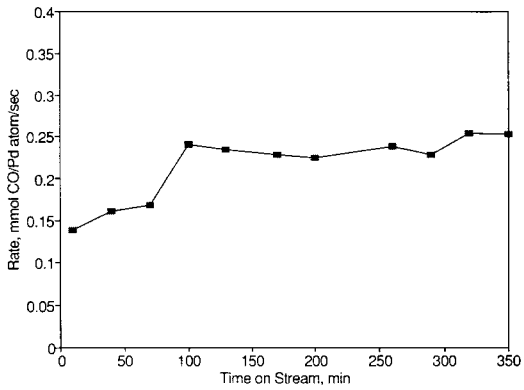

FIG. 1. Activity pattern of Pd_9Co_9 after T_C500/H_2O/T_R250 against time on stream at reaction temperature 250°C.

with TOS for this series are illustrated in Fig. 2 with the Pd_9Co_9 catalyst.

III-a-2. 500/H_2O/500. For catalysts calcined at 500°C and reduced at 500°C, the conversion rates reach a steady state after 2 hr, i.e., earlier than the 500/H_2O/250 condition. As shown in Fig. 3, the conversion rate increases with Co/Pd ratio. The selectivities vs TOS (not shown) are similar to those of the 500/H_2O/250 series (Fig. 2), except for a lower maximum selectivity to MeOH + DME. Figure 4 shows that the selectivity to MeOH + DME decreases with increasing Co/Pd. For Pd_3Co_9, MeOH + DME forma-

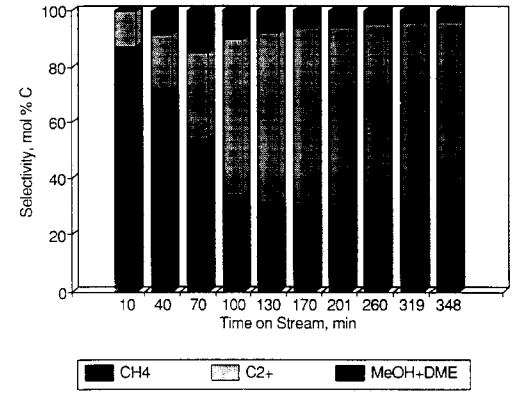

FIG. 2. Selectivity changes of Pd_9Co_9 after T_C500/H_2O/T_R250 against time on stream at reaction temperature 250°C.

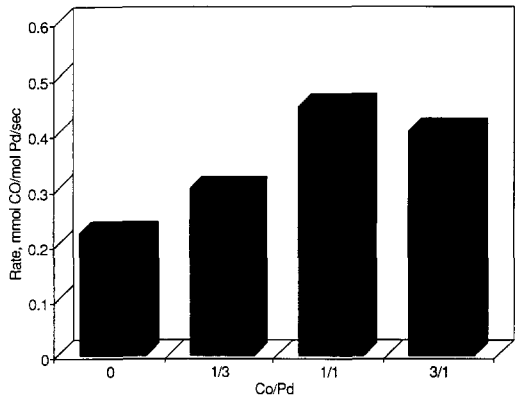

FIG. 3. Steady-state conversion rates of CO (reaction temperature 250°C) of catalysts with various Co/Pd ratios after $T_C500/H_2O/T_R500$.

tion is zero. In addition, the catalysts Pd_9Co_3, Pd_9Co_9, and Pd_3Co_9 show increasing higher hydrocarbons with Co/Pd ratio. A comparison of the higher hydrocarbon distribution on Co-free catalyst Pd_9 and on Co-rich catalyst Pd_3Co_9 is made in Fig. 5. The Co-rich catalyst produces much more low molecular weight higher hydrocarbons but less high molecular weight higher hydrocarbons. Catalysts Pd_3Co_9 and Pd_9Co_9 follow the same trend. The iso/normal ratios of C_4 and C_5 alkanes are higher with Pd_3Co_9 than with Co-free Pd_9.

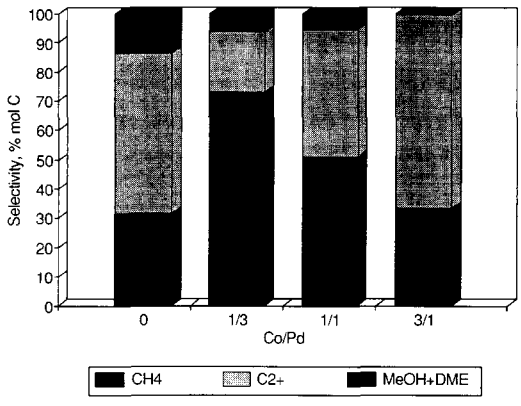

FIG. 4. Steady-state selectivities of catalysts (reaction temperature 250°C) with various Co/Pd ratios and $T_C500/H_2O/T_R500$.

III-a-3. 250/H_2O/350. With this series of catalysts the steady-state activity also increases with Co/Pd ratio (Fig. 6). However, as shown in Fig. 7, the steady-state selectivities are quite different. The Pd_9 and Pd_9Co_3 catalysts show a significantly higher C_{2+} formation at the expense of methane. The Pd_9Co_9 catalyst displays a much higher formation of methane and MeOH + DME, but the formation of C_{2+} is very low. The distribution of the higher hydrocarbon fraction is similar for the Pd_9 and Pd_9Co_3 catalysts.

III-b. X-ray Diffraction

III-b-1. 500/H_2O/250. The full-range X-ray diffraction patterns for the catalyst Pd_9Co_3 of the 500/H_2O/250 series, both before and after syngas reaction at 250°C, are shown in Fig. 8. For comparison, the X-ray diffraction pattern of NaY is also included. The Bragg peaks of NaY, which are corrected with standard Si diffraction peaks, are used to calibrate the Bragg-peak positions of the encaged metal particles in the metal loaded NaY. For the estimation of crystallite size and relative phase abundancy, the NaY peaks are subtracted from those of the catalyst samples. The difference spectrum is also displayed in Fig. 8. Comparison of the XRD patterns of the used catalysts with those before reaction shows a slight decrease of zeolite crystallinity. We ascribe this to the growth of encaged metal particles, and this is confirmed by the electron micrographs (not shown in the present paper). Evidence of local zeolite destruction in absence of water from studies of other reactions in this laboratory suggests that water produced during CO hydrogenation may not be the major cause for the decrease of zeolite crystallinity. Change in crystallinity was taken into account in the NaY background subtraction.

For the freshly prepared catalyst, the diffraction due to metallic phase(s) in the reduced catalyst samples is barely visible, the signal-to-noise ratio of the difference spectrum is extremely poor. This confirms the previous results (*17*) that the NaY-encapsu-

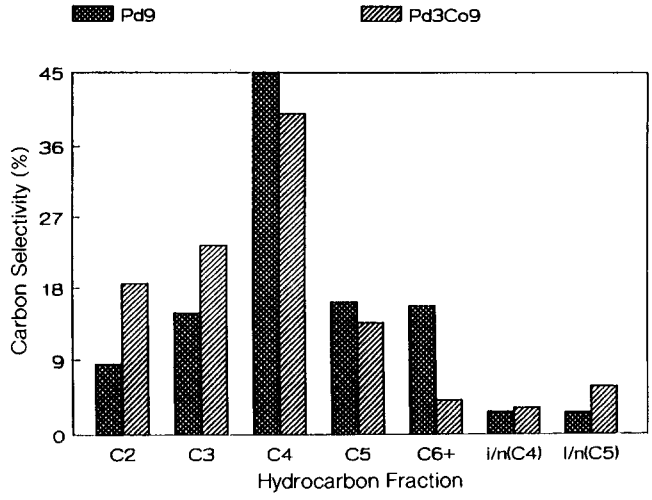

FIG. 5. Higher hydrocarbon distribution on catalysts (reaction temperature 250°C) with various Co/Pd ratios and $T_C500/H_2O/T_R500$.

lated palladium particles are finely dispersed and confined to the cages, they are too small to give XRD patterns.

However, after having been on stream for a couple of hours in syngas conversion, all catalyst samples give distinct XRD peaks, indicating growth of metal crystallites. As all the XRD peaks for the $500/H_2O/250$ catalysts series are similar, we again show the Pd_9Co_3 catalyst as an example. The (111) diffractions due to the metal phases are extracted from the full-range XRD data and shown in Fig. 9. Further quantitative data analysis on the (111) diffraction peak was performed on each metal phase. As shown in Fig. 9, curve deconvolution discerns two phases, $2\theta = 39.10°$ and $2\theta = 39.55°$, both attributed to Pd carbide. The assignment will be further explained in the following section.

III-b-2. $500/H_2O/250$. Catalysts in this series show dramatic changes with the Co/Pd

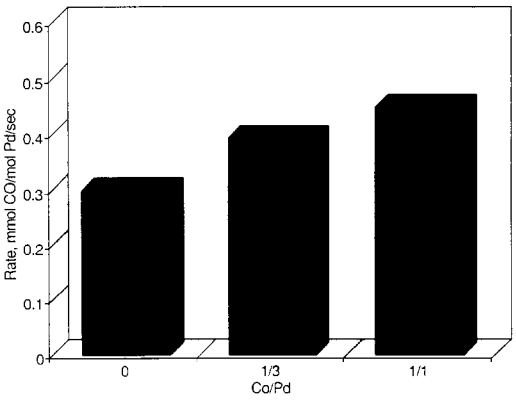

FIG. 6. Steady-state activities of catalysts (reaction temperature 250°C) with various Co/Pd ratios and $T_C250/H_2O/T_R350$.

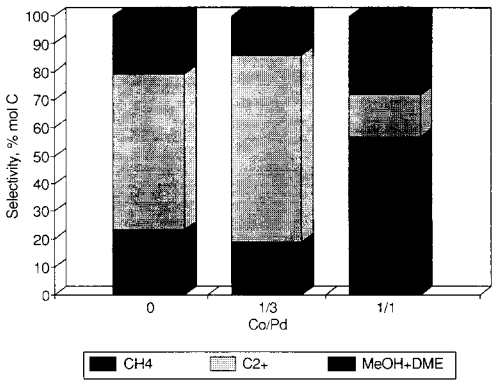

FIG. 7. Steady-state selectivities of catalysts (reaction temperature 250°C) with various Co/Pd ratios and $T_C250/H_2O/T_R350$.

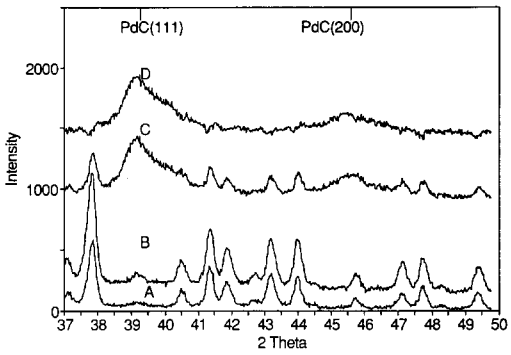

FIG. 8. X-ray diffraction patterns of Pd_9Co_3 (T_C500/H_2O/T_R250) before and after reaction at 250°C. (A) NaY, (B) PdCo before reduction, (C) PdCO after reduction, and (D) C-A.

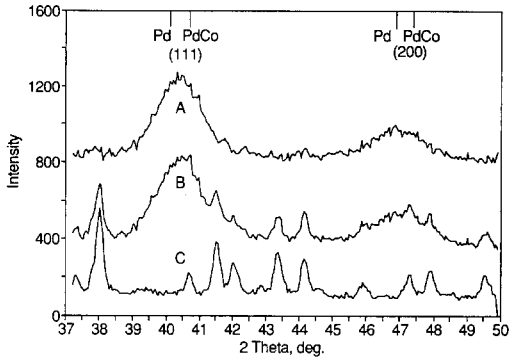

FIG. 10. X-ray diffraction patterns of Pd_9Co_3 (T_C500/H_2O/T_R500) after reaction at 250°C. (A) NaY, (B) Pd_9Co_3, and (C) B-A.

ratio. The full-range X-ray diffraction pattern is displayed in Fig. 10 with only Pd_9Co_3 catalyst as an example. The spectra of the extracted (111) diffraction peaks for this series are illustrated in Fig. 11. Some of the diffraction peaks are rather simple, crystallite sizes can be computed from them by the XRAY12 program developed by Materials Research Center, Northwestern University. But for some envelopes that encompass two distinct metallic phases, deconvolution analysis becomes necessary. One example of such deconvolution is shown in Fig. 11B. The deconvolution program gives directly individual peak positions, FWHM, and intensities of the deconvoluted curves, from which crystallite size and relative phase abundance can be estimated. A correction of FWHM for the separation of the doublet of the K_α radiation, and a refinement in the calculation of true size-broadening, resulting from sample broadening (FWHM) and instrumental broadening (*18*), give only an improvement of less than 10% in crystallite size calculation. As the experimental error of XRD is also of this order, we decide not to include corrections or refinements. The Cauchy–Gaussian curve (*19*) was thus used to calculate true size-broadening at (111) and (200) peaks from observed FWHM and instrumental-broadening. Average crystallite size was calculated from the true size-broadening via the Scherrer equation. The crystallite size calculated from XRD (200) peak broadening are mostly in agreement with those from (111) peak, except in one case the signal/noise ratio of a (200) peak broadening is too low to allow meaningful determination.

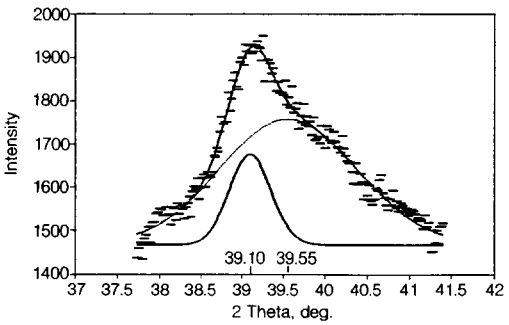

FIG. 9. The (111) X-ray diffraction peak of Pd_9Co_3 (T_C500/H_2O/T_R250) with NaY background subtracted.

While the Co-free Pd_9 catalyst after reaction shows only a Pd carbide phase, shown in Fig. 11A, two phases are detected for Pd_9Co_3 (Fig. 11B). One is pure Pd (trace I) and the other is a PdCo alloy (trace II). With increased Co/Pd ratio as of Pd_3Co_9 (Fig. 11C), only one PdCo alloy phase is detected. Results from quantitative analysis are listed in Table 1.

III-b-3. 250/H_2O/350. The (111) and (200)

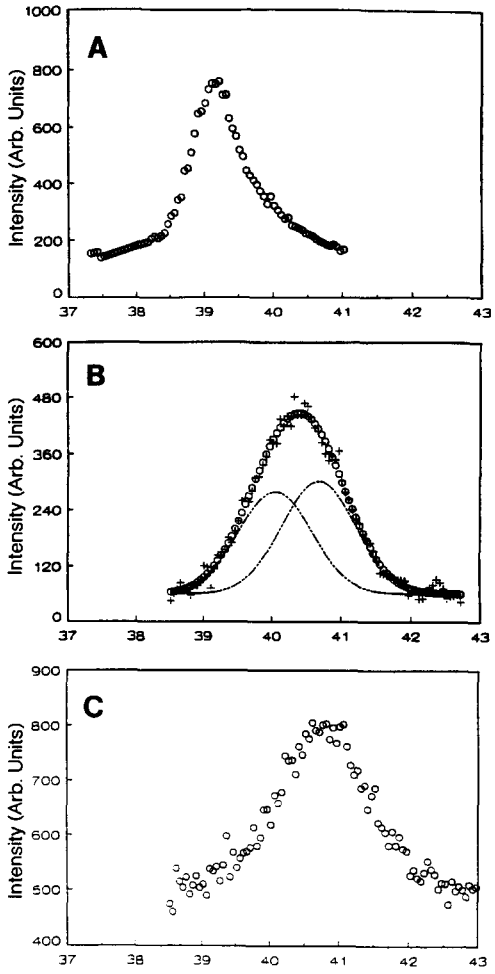

FIG. 11. The (111) X-ray diffraction peak of Pd_9, Pd_9Co_3, and Pd_9Co_9 of $T_C500/H_2O/T_R500$ series with NaY background subtracted: (A) PD_9, (B) Pd_9Co_3, and (C) Pd_9Co_9.

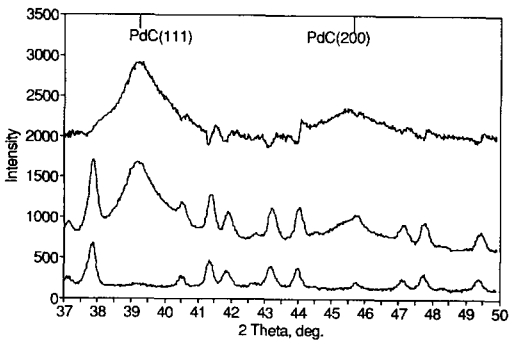

FIG. 12. X-ray diffraction patterns of Pd_9Co_3 ($T_C250/H_2O/T_R350$) after reaction at 250°C. (A) NaY, (B) Pd_9Co_3, and (C) B-A.

diffraction peaks are illustrated by the full-range XRD data in Fig. 12 with catalyst Pd_9Co_3 after reaction as an example. Again, the (111) peaks for all catalysts are analyzed for a quantitative comparison. They are shown in Fig. 13 and Table 2.

Figure 13 and Table 2 show that, after reaction, Pd_9 and Pd_9Co_3 catalysts only contain a Pd carbide phase, while catalyst Pd_9Co_9 contains predominantly Pd metal.

IV. DISCUSSION

The present data show remarkable differences in catalytic selectivity and activity in syngas conversion, not only for samples of different Co/Pd composition, but also among samples of equal composition but different preparation history. We show that these differences can be attributed to the formation of Pd carbide and PdCo alloy par-

TABLE 1

Particle Sizes (nm) from XRD of $500/H_2O/500$ Series after Reaction

Phases	Pd_9	Pd_9Co_3	Pd_9Co_9	Pd_3Co_9[a]
PdC	11.3 (39.16)	—	—	—
Pd	—	7.0 (40.05)	—	—
PdCo	—	6.7 (40.68)	5.8 (40.73)	—
Pd/PdCo phase ratio		0.9		

Note. The numbers in parenthesis are 2θ values. The last line gives the phase ratio from deconvoluted results.
[a] The peak from subtraction is too diffuse and the intensity is too low to allow location a of peak position.

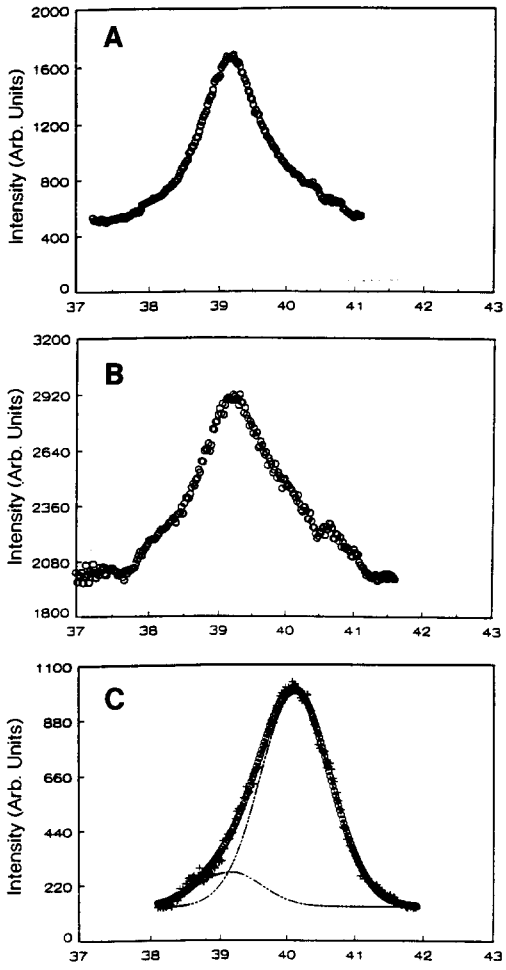

FIG. 13. The (111) X-ray diffraction peak of Pd_9, Pd_9Co_3, and Pd_9Co_9 of $T_C250/H_2O/T_R350$ series (NaY background subtracted): (A) Pd_9, (B) Pd_9Co_3, and (C) Pd_9Co_9.

ticles, respectively. In this interpretation use is made of the present XRD data and of our previous results which show that the formation of PdCo alloy depends crucially on the calcination and reduction conditions. This latter dependence had been analyzed in previous papers, showing that the mutual proximity of Co and Pd ions prior to reduction is a decisive factor, which can be controlled by the calcination temperature. Under the conditions used in the present work Pd may be assumed to be completely reduced, but the reduction of Co will be incomplete and critically dependent on the conditions of calcination and reduction. All samples were exposed to moist air after calcination and prior to reduction. Color changes during this exposition indicate that metal ions inside the zeolite become hydrated, the duration of this treatment was sufficient to reach saturation and constant color.

For the samples reduced at 250°C the reduction of cobalt is minimal. Accordingly, activity and selectivity of the $500/H_2O/250$ catalysts are very similar and independent of the Co loading. They all exhibit the catalytic signature of Pd at identical pretreatment conditions. The XRD patterns after reaction also confirm the similarity of the active metal phase in these catalysts. The peaks deconvoluted from PdC_x (111) envelope differ in FWHM, suggesting that the rates of carburization and agglomeration of the Pd metal particles are mutually dependent.

For this series of catalysts the (111) and (200) X-ray diffraction peaks of palladium (2θ = 40.114° and 46.661°) usually both shift to lower 2θ values with extended time on stream, showing lattice expansion of the Pd particles. As Pd hydrides would decompose under the conditions to which these samples have been exposed before the XRD patterns were taken, we attribute the lattice expansion to the formation of a solid solution with interstitial carbon atoms in the Pd lattice, in agreement with data by Ziemecki *et al.* (*20*, *21*). These authors showed by Rietveld refinement of neutron diffraction data that the PdC_x lattice with 2θ = 39.10 is stable and contains 13 atom% carbon. Ziemecki *et al.* also report that for their samples CO would dissociate and form Pd carbide only at elevated temperature, e.g., 500°C. It is interesting that in the present samples this process is already observed at 250°C. This enhanced reactivity of Pd is obviously due to the much smaller initial particle size. Our previous EXAFS data show that the Pd particles in NaY initially consist of 1–6 atoms only (*17*,

TABLE 2

Particle Sizes (nm) from XRD of 250/H_2O/350 Series after Reaction

Phases	Pd_9	Pd_9Co_3	Pd_9Co_9	Pd_3Co_9[a]
PdC	8.5 (39.12)	5.5 (39.24)	7.8 (39.14)	—
Pd	—	—	7.1 (40.12)	—
PdCo	—	—	—	—
PdC/Pd phase ratio			0.15	

Note. The numbers in parenthesis are 2θ values. The last line gives the phase ratio from deconvoluted results.

22). When these particles are exposed to CO they migrate and coalesce as has been demonstrated by EXAFS (*17*, *22*). Under these circumstances CO dissociation and carbide formation are prevailing, as indicated earlier by the high initial selectivity for CH_4 formation, which is again confirmed in the present work. The formation of Pd carbides, instead of Pd hydrides, was explicitly confirmed by treating the used catalyst in H_2 for 16 hr. This led to formation of CH_4 detected by gas analysis, while simultaneously the carbides reverted to Pd, as shown by XRD (*4*).

In Fig. 9, the (111) peak appears to be a composite reflection from different phases. Although a broad range of carbon concentrations might exist in the Pd lattice, the simplest approach based on an inspection of the peak envelope indicates the presence of two palladium carbide phases of different carbon concentrations. Other authors also found the splitting of the X-ray diffraction line due to Pd(111) into two components and suggested it to be due to the coexistence of two palladium carbide phases with different extent of lattice expansion (*20*, *21*, *23*).

Kepinski and Wolcyrz (*24*, *25*) showed that alloying with other metals such as Si and Al prevents the carburization of Pd. For the present Pd–Co system, it is evident that a small fraction of reduced Co is sufficient to suppress the formation of Pd carbide as is the case for Pd_9Co_9 of the 250/H_2O/350 series (Fig. 13C). After T_C = 250°C, only 12% of the Co^{2+} ions in Pd_9Co_9 can be reduced at 450°C limited by the scarce population of Co^{2+} ions in supercages. At T_R = 350°C, the extent of Co^{2+} ion reduction is extremely small as follows from the temperature programmed reduction profile (*13*). Obviously, the amount of reduced Co in Pd_9Co_3 after 250/H_2O/350 is too low to prevent Pd carbide formation as shown in Fig. 13(B). Using X-ray and electron diffraction studies, Bozorth *et al.* (*26*) and Matsuo (*27*, *28*) demonstrated that Pd and Co form a continuous series of solid solutions. The lattice constant vs composition line is slightly curved upwards. Therefore, the Co content in the Pd–Co alloy particle can be estimated from the position of (111) diffraction peak of the Pd–Co alloy particles. The Co contents obtained in this way for the alloy particle in Pd_9Co_3 500/H_2O/500, and Pd_9Co_9 500/H_2O/500 are 18 and 21 atom%, respectively. Since the X-ray diffraction patterns are determined for catalysts after extended periods on-stream, this information is relevant to the steady state of the catalysts. Only one PdC phase exists in all catalysts of the 500/H_2O/250 series with an average particle size of 5.5 to 8.5 nm. We note that similar structures correlate with similar activity and selectivity of these samples.

For the 500/H_2O/500 series after reaction, XRD patterns in Fig. 11 demonstrate the formation of $PdCo_x$ alloy particles with average sizes of 6–7 nm, both for the Pd_9Co_3 and the Pd_9Co_9 catalysts. While the Pd loading is constant, e.g., Pd_9, the extent of Co^{2+} reduction increases with the Co/Pd ratio (*13*). As a result, alloying of Pd with Co becomes complete and PdCo becomes pre-

dominant in the Pd_9Co_9 catalyst, whereas Pd metal and PdCo alloy phases coexist in Pd_9Co_3.

The increase of the catalytic conversion rate per Pd atom with increasing Co/Pd ratio in the 500/H_2O/500 series as shown in Fig. 3 can therefore be attributed to an increased Co content of the $PdCo_x$ alloy particles. A comparison of the traces B and C in Fig. 11 suggests that, in addition to the increased Co concentration in the alloy, the number of PdCo alloy particles is much greater in Pd_9Co_9 than in Pd_3Co_9, since the envelopes of the two (111) peaks are of nearly the same intensity.

As the rates shown in Fig. 3 are those at the end of the test run, the lower value for the Pd_3Co_9 catalyst compared to that of Pd_9Co_9 indicates a faster deactivation of the former. At the end of the reaction, the activity of Pd_9Co_9 has decreased by 20% from the initial activity, but that of Pd_3Co_9 has decreased by 40%. It thus appears that the increased Co concentration in the PdCo alloy particles leads to faster deactivation. Unfortunately, the amount of metal in the reduced phase is very low for Pd_3Co_9 so that XRD analysis suffers from a poor signal to noise ratio. The XRD peak as shown in Fig. 11A shows, however, that for the Co-free Pd_9 catalyst only PdC_x is abundant. Likewise, its selectivity as shown in Fig. 4 is very similar to that of other catalysts containing only PdC_x.

While it is known that Pd is a good methanol synthesis catalyst, alloying Pd with Co decreases the selectivity to methanol. It is particularly interesting to note that a very small amount of reduced Co not only protects the Pd metal against carbide formation, but also leads to an increased methane selectivity in comparison with the Co-free catalysts. This holds for Pd_9Co_3 in the 500/H_2O/500 series (for selectivity see Fig. 4 and for Pd phase, see Fig. 11B, trace I) and also for Pd_9Co_9 in 250/H_2O/350 (selectivity in Fig. 7 and Pd phase in Fig. 13C). As discussed above, the fraction of Co reduced in the 250/H_2O/350 series is low, even though the Co loading is higher in Pd_9Co_9 than in Pd_9Co_3. The rates of carbide cleaning and methanation are likely related with each other. The overall rate of CO dissociation followed by hydrogenation of C atoms will be faster on mixed $PdCo_x$ ensembles than on pure Co or Pd ensembles. Isolated Co atoms decorating the Pd particles might also provide a faster methanation rate so that carbide precursors are removed by Co. An alternative mechanism supposes that the decorating Co atoms hydrogenate methanol formed on Pd sites.

It is interesting to note that the selectivity to higher hydrocarbons increases with increasing formation of PdCo alloy in the 500/H_2O/500 series (Fig. 11), as shown in Fig. 4. In fact Pd_3Co_9 gives more higher hydrocarbons than Pd_9. Such change at first seems peculiar because the PdC_x phase in Pd_9 and the PdCo phase in the catalysts with higher Co/Pd ratios both show high hydrocarbon selectivity. These phases differ, however, in the distributions of higher hydrocarbons, as displayed in Fig. 5. When the Co/Pd ratio increases, there is a gradual shift in the product distribution from heavier hydrocarbons such as C_{6+} to the lighter hydrocarbons such as C_2 and C_3. While the product distribution favoring heavier hydrocarbons on the Pd_9 catalyst of this series is in good agreement with our previously reported results (*4*), an increasing Co/Pd ratio evidently shifts the product distribution toward normal Fischer–Tropsch behavior. Different mechanisms contribute to the formation of higher hydrocarbons. On PdC_x methanol formation is the prevailing process, as shown in our previous papers. The observed higher hydrocarbons are due to secondary reactions of methanol and dimethyl ether on strong Brønsted-acid sites. The product distribution of the secondary reaction favors heavier hydrocarbons. A second mechanism is the Fischer–Tropsch process, starting with CO dissociation and characteristic for Co catalysts. The bimetal PdCo catalysts differ from the PdNi cata-

lysts in their methanation selectivities. Whereas, an increasing extent of alloying Co with Pd favors C_{2+} hydrocarbons, alloying of Ni with Pd selectively produces methane (*9*).

The similar product distribution for Pd_9 and Pd_9Co_3 in the $250/H_2O/350$ series is not surprising because both catalysts contain PdC_x as the active catalytic phase. The low Co reduction in Pd_9Co_3 is in good agreement with our previous study of Co^{2+} reduction (*13*). The increased Co loading in the Pd_9Co_9 catalyst leads to slightly higher Co^{2+} ion reduction, which is, however, insufficient to form a PdCo alloy phase detectable by XRD, but sufficient to suppress carbide formation. Incipient alloy formation may be responsible for the enhanced selectivity towards methane.

V. CONCLUSIONS

(1) While the presence of small particles undetectable by XRD and of deviating composition can never be excluded, the present data show that observed catalytic activity and selectivity results can be reasonably correlated with the presence of either Pd carbide or PdCo alloys or both, which are clearly identified by XRD.

(2) Formation of methanol, eventually followed by condensation to dimethyl ether and formation of higher hydrocarbons on acid sites, is the characteristic signature of catalysts containing Pd or Pd carbide after agglomeration of the original particles which dissociate CO and form methane.

(3) Alloying Pd with Co suppresses formation of Pd carbide and enhances formation of hydrocarbons initiated by dissociative adsorption of CO. More surface sites on Co-rich alloys catalyze formation of higher hydrocarbons with distribution reminiscent of Co catalysts used in Fischer–Tropsch synthesis.

(4) The reduction of Co^{2+} and the formation of $PdCo_x$ alloys is controlled by the Co content, the proximity of Co and Pd ions, and the reduction temperature in a manner elucidated in previous papers.

ACKNOWLEDGMENTS

We gratefully acknowledge support from the Director of the Chemistry Division, Basic Energy Sciences, U.S. Department of Energy, Grant DE-FGO2-87ERA13654. Thanks are due to Mr. M. S. Shih, Department of Physics, Northwestern University, for his kindness in providing the deconvolution program for X-ray diffraction peaks.

REFERENCES

1. Zhang, Z., Cavalcanti, F. A. P., and Sachtler, W. M. H., *Catal. Lett.* **12,** 157 (1992).
2. Poutsma, M. L., Elek, L. F., Ibarbia, P. A., Risch, A. P., and Rabo, J. A., *J. Catal.* **52,** 157 (1978).
3. Driessen, J. M., Poels, E. K., Hindermann, J. P., and Ponec, V., *J. Catal.* **82,** 26 (1983).
4. Cavalcanti, F. A. P., Stakheev, A. Yu., and Sachtler, W. M. H., *J. Catal.* **134,** 226 (1992).
5. Fujimoto, K., Kudo, Y., and Tominaga, H., *J. Catal.* **87,** 136 (1991).
6. Thomson, R. T., and Wolf, E. E., *Appl. Catal.* **41,** 65 (1988).
7. Guzci, L., *in* "Catalysis 1987," (J. W. Ward, ed.), p. 85. Elsevier, Amsterdam, 1988.
8. Choudary, B. M., Lazar, K., Matusek, K., and Guczi, L., *J. Soc. Chem. Commun.*, 592 (1988).
9. Feeley, J. S., Stakheev, A. Yu., Cavalcanti, F. A. P., and W. M. H., Sachtler, *J. Catal.*, in press.
10. Fornasari, G., La Torretta, T. M. G., Vaccari, A., Bednarova, S., Jirů, P., and Tvaruzkova, Z., *Stud. Surf. Sci. Catal.* **61,** 333 (1990).
11. Nazar, L. F., Ozin, G. A., Hugues, F., and Godber, J., *J. Mol. Catal.* **21,** 313 (1983).
12. Wang, W. J., and Chen, Y. W., *Appl. Catal.* **77,** 21 (1991).
13. Zhang, Z., Sachtler, W. M. H., and Suib, S. L., *Catal. Lett.* **2,** 395 (1989).
14. Suzuki, M., Tsutzumi, K., Takahashi, H., and Saito, Y., *Zeolites* **8,** 381 (1988).
15. Zhang, Z., and Sachtler, W. M. H., *J. Chem. Soc. Faraday Trans.*, **86,** 2313 (1990).
16. Karpíński, Z., Zhang, and Sachtler, W. M. H., *Catal. Lett.* **13,** 123 (1992).
17. Zhang, Z., Chen, H., L. L., and Sachtler, W. M. H., *J. Catal.* **127,** 213 (1991).
18. Alexander, L. E., *J. Appl. Phys.* **25,** 155 (1954).
19. Jones, F. W., *Proc. R. Soc. London Ser. A.* **166,** 16 (1938).

20. Ziemecki, S. B., and Jones, G. A., *J. Catal.* **95,** 621 (1985).
21. Ziemecki, S. B., Jones, G. A., Swartzfager, D. G., Harlow, R. L., and Faber, J., Jr., *J. Am. Chem. Soc.* **107,** 4547 (1985).
22. Zhang, Z., Chen, H., and Sachtler, W. M. H., *J. Chem. Soc. Chem. Commun.* **87,** 1413 (1991).
23. Zaidi, A. H., *Appl. Catal.* **30,** 131 (1987).
24. Kepinski, L., and Wolcyrz, M., *Appl. Catal.* **54,** 267 (1989).
25. Kepinski, L., and Wolcyrz, M., *Appl. Catal.* **73,** 173 (1991).
26. Bozorth, R. M., Wolff, P. A., Davis, D. D., Compton, V. B., and Wernick, J. H., *Phys. Rev.* **122,** 1157 (1961).
27. Matsuo, Y., *J. Phys. Soc. Jpn.* **28,** 1375 (1970).
28. Matsuo, Y., *J. Phys. Soc. Jpn.* **32,** 972 (1972).